Global Journal of Engineering and Technology Advances
eISSN: 2582-5003
Cross Ref DOI: 10.30574/gjeta
Journal homepage: https://gjeta.com/

(RESEARCH ARTICLE)

Check for updates

Corrosion Inhibition and Process Optimization of AISI 4140 Alloy Steel in 15% HCl Using *Newbouldia laevis* (Ogirisi) Leaves: RSM-OCD Approach

Augustine U. Iwuoha [1], Obiora Clement Okafor [1,*], Ibeje Andy Obinna [2] and Mercy Chinenye Iroegbu [3]

[1] *Department of Mechanical Engineering, Imo State University, Owerri, Nigeria.*
[2] *Department of Civil Engineering, Imo State University, Owerri, Nigeria.*
[3] *Department of Electrical and Electronic Engineering, Imo State University, Owerri, Nigeria.*

Global Journal of Engineering and Technology Advances, 2026, 26(03), 081-101

Publication history: Received on 20 January 2026; revised on 06 March 2026; accepted on 06 March 2026

Article DOI: https://doi.org/10.30574/gjeta.2026.26.3.0048

Abstract

The corrosion of AISI 4140 alloy steel tubing during oil and gas well acidizing with 15% HCl poses a major challenge. This study assessed the inhibitory performance of *Newbouldia laevis* (NBL) leaf extract on AISI 4140 alloy steel in 15% HCl by integrating mass-loss experiments, electrochemical impedance spectroscopy (EIS), and potentiodynamic polarization (PDP) measurements, and scanning electron microscopy (SEM). The NBL leaf extract was prepared by Soxhlet extraction with ethanol and characterized for its phytochemical constituents. A 16-run Optimal Custom Design (OCD) was generated with immersion time (2, 4, & 6 hrs.), NBL concentration (4, 5 and 6 g/L), and temperature (303, 323 and 353 K) as factors, and corrosion rate and inhibition efficiency as responses. Inhibitor concentrations and operating conditions were optimized via Response Surface Methodology-Optimal Custom Design (RSM-OCD). Phytochemical analysis confirmed the presence of flavonoids (most abundant), phenols, tannins, steroids, terpenoids, and glycosides. RSM-OCD optimization identified the optimal conditions of 2 h, 6 g/L NBL concentration, and 303 K, predicting a corrosion rate of 1.256 mm/yr and inhibition efficiency of 94.056%. PDP results showed NBL functions as a mixed-type inhibitor with maximum inhibition efficiency of 89.42% at 7 g/L. EIS confirmed a maximum inhibition efficiency of 88.31% at 7 g/L. SEM revealed a dense heterogeneous protective film formed by 6 g/L NBL. Therefore, we recommend NBL leaf extract as a viable, sustainable, and eco-friendly corrosion inhibitor for protecting steel tubing during acidizing operations in the oil and gas industry.

Keywords: AISI 4140 Alloy Steel; *Newbouldia Laevis* Leaves; Corrosion; Green Inhibition; Electrochemical Measurements; Gravimetric Measurements

1. Introduction

Steel corrosion is a major challenge across many industries, arising naturally at the metal–solution interface and significantly shortening the service life of equipment and tools. Moreover, corrosion can promote the release of toxic metals from structures and machinery [1–3]. In response, various organic molecules have been identified as effective corrosion inhibitors for metals and alloys [4–6]. Experimental evidence shows that when these organic molecules adsorb onto the metal surface, they alter the interfacial properties and disrupt corrosive reactions, thereby efficiently inhibiting corrosion [7] and reducing reliance on expensive, often environmentally harmful synthetic inhibitors [8].

AISI 4140 steel, an alloy composed primarily of iron and carbon, with chromium and molybdenum as key alloying elements, is widely used in the oil and gas industry for downhole tools and wellhead components. To boost oil production, wells are commonly acidized by injecting a solution of 15–28% hydrochloric acid (HCl) through steel tubing

* Corresponding author: Obiora Clement Okafor

[9]. This process creates channels in the rock formation to enhance oil flow, and HCl is favored for its strong rock-dissolving ability and cost-effectiveness [10, 11].

Additionally, because HCl accelerates corrosion of tubing and casing materials, inhibitors are added to the acid during acidization to protect steel surfaces [12–15]. Most oilfield corrosion inhibitors are organic compounds featuring oxygen, nitrogen, sulfur, multiple bonds, or heterocyclic and aromatic rings in their molecular structures [16]. Molecules with lone pairs or π-electrons exhibit strong adsorption to metal surfaces [17–20], and heterocyclic compounds containing oxygen, nitrogen, sulfur, and unsaturated bonds are particularly effective corrosion inhibitors [21]. Compounds with nitrogen-containing heterocycles have demonstrated especially high inhibition efficiency in steel–acid systems [22, 23].

The growing environmental awareness and stricter regulations have driven the search for sustainable "green" corrosion inhibitors [24]. In this regard, plant extracts have been extensively studied as eco-friendly alternatives [25–28]. For example, pharmacological and physicochemical investigations of NBL have revealed its rich content of flavonoids, alkaloids, and tannins, with alkaloids exhibiting analgesic activity [29]. NBL has also been shown to possess antimicrobial and antioxidant properties and is used to treat various ailments [27]. Additionally, previous studies have explored the efficacy of NBL extracts in mitigating steel corrosion in both sulfuric and hydrochloric acid media. In one gravimetric study [30], ethanol refluxed leaf extracts were tested at concentrations from 0.1 to 0.5 g/L in 1 M H_2SO_4. Mild steel coupons immersed for up to 20 h exhibited a marked decrease in weight loss, from 0.173 g (no inhibitor) to 0.017 g (0.5 g/L), and a corresponding reduction in corrosion rate from 43 mm yr^{-1} to 4.2 mm yr^{-1}. Inhibition efficiencies rose from 72% to 90% with increasing extract concentration. A similar investigation [31] confirmed these findings: at 0.1 g/L and 0.5 g/L, inhibition efficiencies reached 88% and 93% respectively, after 20 h in 1 M H_2SO_4. Another weight loss study [32] showed that ethanol extracts of NBL leaves effectively inhibited corrosion of high carbon steel in 1 M sulphuric acid over 20 hours. The extract reduced corrosion rates significantly, with inhibition efficiency increasing with concentration: 88% at 0.1 g/L and a maximum of 93% at 0.5 g/L after 20 hours. These results confirm a clear concentration-dependent protective effect, highlighting the extract's potential as an efficient, eco-friendly corrosion inhibitor in acidic media.

Collectively, these results demonstrate that NBL leaf extract significantly extends the service life of carbon steels in acidic medium. Extending the inquiry to hydrochloric acid, stem bark and leaf extracts of NBL were evaluated in 0.5 M HCl [33]. After six hours at 309 K, the stem bark extract achieved an inhibition efficiency of 85%, while the leaf extract reached 76.7%. Adsorption behavior followed Langmuir, Temkin, and Adejo Ekwenchi isotherms, indicating chemisorption as the dominant mechanism. These studies collectively establish NBL extracts as potent, green corrosion inhibitors for mild steel in acidic environments, offering a sustainable alternative to conventional synthetic inhibitors.

Therefore, optimizing inhibitor concentration and process parameters through the RSM-OCD technique is critical to maximizing the efficacy of plant-derived extracts. Moreover, elucidating the corrosion behavior of AISI 4140 steel tubing in highly acidic environments (15 % HCl)- which is the typical condition used in oil and gas well acidization operation and quantifying the protective effect of NBL extract will both deepen the mechanistic understanding and accelerate the adoption of bio-based corrosion inhibitors. In this work, we assessed the inhibitory performance of NBL leaf extract on AISI 4140 alloy steel in 15 % HCl by integrating mass-loss experiments, electrochemical impedance and polarization measurements, and scanning electron microscopy (SEM). Inhibitor concentrations and operating conditions were systematically optimized via an RSM-OCD method, ensuring a data-driven path to robust, sustainable corrosion protection.

2. Materials And Method

The NBL leaves depicted in Figure 1a were collected from Anupama Village, in Oba, located in Ide Mili-South Local Government Area of Anambra State, Nigeria. Prior to use, the leaves were thoroughly washed to eliminate sand and other impurities and subsequently sun-dried for eight (8) days to prepare them for the extraction of corrosion-inhibiting constituents as presented in Figure 1b. Additionally, three (3) AISI 4140 steel tubing samples, each measuring 590 mm in length, with an external diameter of 25 mm and an internal diameter of 20 mm, as illustrated in Figure 2, were procured from Dashing Company, China, and imported into Nigeria for this study. To confirm the material's chemical composition and ensure consistency with the accompanying material data chart, the steel samples were analyzed using an Atomic Emission Spectroscopy (AES) system.

Figure 1 The leaves of NBL (a) freshly plucked from the tree (b) under sun-drying process

Figure 2 Image of AISI 4140 alloy steel tubing

2.1. Formulation of the NBL-Based Inhibitor

The materials used for the extraction process included a 500 mL capacity heating mantle, measuring cylinder, analytical balance, semi-permeable membrane, 500 mL quick-fit Soxhlet extraction system, ethanol, water circulation tubes, and a rotary evaporator. The sun-dried NBL leaves were pulverized using a 650W electric blender and stored in clean, moisture-free containers in preparation for Soxhlet extraction. A 30 g portion of the ground and sieved sample was weighed, wrapped in cotton fabric, and inserted into the thimble of a 500 mL Soxhlet extractor. The Soxhlet apparatus consisted of a thimble, a condenser, and a 500 mL flat-bottom round flask. A 250 mL volume of ethanol was measured and poured into the round-bottom flask. The Soxhlet setup, containing the sample enclosed in the semi-permeable membrane, was assembled and connected to the condenser, which was fitted onto the flask containing ethanol. The system was heated to 80 ℃ using the heating mantle, while water was continuously circulated through the condenser's jacket to ensure efficient condensation. Extraction continued until the phytochemical constituents were fully extracted. The spent residue in the membrane was then discarded. Subsequently, the ethanol–phytochemical mixture in the round-bottom flask was subjected to distillation in a water bath maintained at 80 ℃. During the process, ethanol was evaporated and collected separately, leaving the concentrated phytochemical extract in the flask. The final extract was sealed in an air-tight container and stored under cool, dry conditions. The NBL leaf extract obtained via Soxhlet extraction, and its various concentrations used in this study are delineated in Figure 3.

Figure 3 NBL inhibitor securely kept inside an airtight container (a) just as extracted from the Soxhlet machine (b) prepared to solutions of 4, 5, and 6g/l

2.2. Preparation of Test Samples from AISI 4140 Steel Tubing

The test specimens were cut and machined into rectangular coupons with dimensions of 25 mm × 20 mm × 0.5 mm for gravimetric analysis, and 2 cm × 2 cm × 0.5 cm for electrochemical impedance spectroscopy (EIS) and potentiodynamic polarization (PDP) evaluations as displayed in Figure 4. The elemental composition of the base material was determined using an AES analyzer to verify material conformity. Surface preparation was performed by sequential polishing with emery papers of varying grit sizes (800 and 220) to ensure a smooth and uniform metallic surface for accurate corrosion assessment. The polished samples were then degreased with acetone to remove residual oils or organic impurities, thoroughly rinsed with distilled water, air-dried, and stored in a desiccator to prevent oxidation and environmental contamination. Each coupon's initial weight was recorded using a high-precision electronic analytical balance to facilitate accurate post-exposure measurements.

Figure 4 Some of the prepared samples used for the corrosion assessment tests

2.3. Preparation of the Corrosive Medium

In this investigation, a 15% hydrochloric acid (HCl) solution, commonly utilized in oil well acidization processes, was prepared from an analytical-grade stock solution. The concentrated HCl had an initial concentration of 35%, a density of 1.18 g/cm^3, and a molar mass of 36.46 g/mol. The dilution was carried out using the standard dilution equation, as shown in Equation (1), to achieve the target concentration. Based on the calculated proportions, a 2000 mL solution of 15% HCl (equivalent to 4.42 M) was obtained by mixing 780 mL (920 g) of the 35% HCl stock solution with 1220 mL (1220 g) of distilled water.

$$C_1V_1 = C_2V_2$$

Where: C_1 = initial concentration of HCl (35% or 11.33 M), V_1 = volume of 35% HCl solution required, C_2 = desired concentration of HCl (15% or 4.42 M), V_2 = final volume of 15% HCl solution = 2000 ML.

2.4. Qualitative and Quantitative Phytochemical Analysis of NBL

Phytochemical analysis of the NBL extract was performed using both qualitative and quantitative approaches. The qualitative analysis confirmed the presence or absence of specific phytochemical constituents, while the quantitative evaluation provided precise measurements of their concentrations. These analyses were meticulously carried out following established protocols as outlined in the literature [34-37]. The primary phytochemicals examined in the NBL extract included phenols, flavonoids, saponins, alkaloids, tannins, terpenoids, glycosides, and steroids.

2.5. D-Optimal Experimental Design (DoE)

The experimental framework was constructed using the Optimal Custom Design (OCD) module, a specialized subset of RSM integrated within Design Expert Software v13.0. This methodology provides a highly flexible design structure capable of accommodating custom models, categorical variables, and irregular or constrained experimental regions. The selection of experimental runs was determined based on predefined selection criteria established during the model-building phase. In this study, time was designated as a fixed numeric factor, while NBL concentration and temperature were treated as categorical variables. These three parameters served as the independent (input) factors, with corrosion rate (CR) and inhibition efficiency (IE) defined as the dependent response variables. To efficiently explore the design space, the "Both Exchanges" search algorithm, combining Point Exchange and Coordinate Exchange strategies, was employed. The OCD methodology is based on D-optimality, which produces a design that best estimates the effects of the factors on responses. The algorithm picks points that minimize the volume of the confidence ellipsoid for the coefficients. The mathematical constraints and inequalities guiding the formulation of this design space are delineated accordingly. The final experimental matrix, consisting of 16 design runs, is summarized in Table 1.

$$303 \leq \text{Temperature} \leq 353$$

$$4 \leq \text{NBL concentration} \leq 6$$

$$2\text{hrs.} \leq \text{Time} \leq 6\text{hrs}$$

Table 1 Experimental design (DoE)

	Factor 1	**Factor 2**	**Factor 3**
Run	**A: Time**	**B: NBL concentration**	**C: Temperature**
	Hrs.	g/l	K
1	4	5	303
2	5	4	303
3	2	6	303
4	3	6	353
5	6	4	323
6	3	4	323
7	6	5	323
8	2	5	353
9	6	6	353
10	2	4	353
11	2	6	323
12	2	5	303
13	5	4	353
14	6	6	303
15	5	6	323
16	6	5	353

2.6. Corrosion Assessment Using the Gravimetric Method

The corrosion behavior of AISI 4140 steel coupons in 15% HCl solution and the inhibitory effectiveness of NBL were evaluated using the weight loss method, following the experimental design detailed in Table 1. Each experimental condition specified in the design of experiments (DoE), including temperatures of 303 K, 323 K, and 353 K, NBL concentration, as well as defined exposure durations, was systematically examined under two distinct scenarios: in the absence of the inhibitor (blank) and the presence of NBL at varying concentrations. Prior to immersion, the steel coupons (2.5cm ×2cm×0.5cm) were accurately weighed using a high-precision electronic balance (±0.01 mg accuracy), in accordance with ASTM G31-72 guidelines [38]. The samples were then immersed in 100 mL of 15% HCl solution without any inhibitor. Following the specified exposure period, the coupons were removed, gently brushed to eliminate corrosion residues, dried using a hot air blower, and reweighed to determine material loss. The procedure was subsequently repeated for each of the three NBL inhibitor concentrations: 4.0 g/L, 5.0 g/L, and 6.0 g/L, ensuring consistency across all test parameters both in the presence and absence of the inhibitor. From the recorded weight loss values, key corrosion metrics, including corrosion rate (CR), inhibition efficiency, and surface coverage, were computed using Equations 2-4 [39].

$$CR = \frac{87.6\Delta W}{\rho A t}$$

$$\eta\% = \frac{Cr_1 - Cr_2}{Cr_1} \times 100$$

$$\theta = \frac{Cr_1 - Cr_2}{Cr_1}$$

Where: ΔW = weight loss after immersion in the absence and presence of various concentrations of NBL (mg), ρ = density of the material (g/cm3), A = cross-sectional area of the material (cm2), t = exposure time in the corrosive medium (hrs.), Cr_1 = corrosion rate in the absence of inhibitors (mm/yr.), Cr_2 = corrosion rate in the presence of inhibitors (mm/yr.).

2.7. Response Optimization Using RSM-OCD

To identify the optimal combination of experimental factors for achieving the most favorable response outcomes, RSM-OCD was employed for process optimization. The optimization strategy strictly adhered to the predefined criteria and target objectives presented in Table 2. Additionally, an Analysis of Variance (ANOVA) was conducted to quantify both the main and interaction effects of the independent variables on the measured responses. This statistical evaluation facilitated the determination of which input factor (regressor) had the most significant positive or negative impact on the corrosion rate (CR) and inhibition efficiency (IE). ANOVA was executed at a 95% confidence interval, corresponding to a significance level of 5%.

Table 2 RSM optimization goals

S/N	Factors	Criteria/goal
1	TA concentration	In-range
2	Temperature	In-range
3	Time	In-range
4	CR	Minimize
5	IE	Maximize

2.8. SEM Examination

Scanning electron microscopy (SEM) was employed to investigate the surface morphology changes on AISI 4140 steel caused by corrosion in a highly aggressive acidic environment and to assess the corrosion inhibition performance of Newbouldia laevis (NBL) extract. This method provided high-resolution images of the surface topography, enabling clear observation of the degree of corrosion attack and the presence of any protective film formed through inhibitor adsorption. Steel specimens were exposed to 15% HCl at 353 K for 6 hours under two conditions: (i) the blank (uninhibited) solution and (ii) the solution containing the optimum inhibitor concentration of 6 g/L NBL. The surface

morphologies obtained in both cases were imaged at 300× magnification and directly compared to reveal differences in surface roughness, pit formation, cracking, and the extent of protective layer coverage.

2.9. EIS and PDP Studies

Electrochemical measurements were conducted using a Potentiated/Galvano stat 263A electrochemical workstation coupled with a conventional three-electrode corrosion cell setup. A graphite rod served as the counter electrode, a saturated calomel electrode (SCE) as the reference electrode, and polished AISI 4140 steel coupons prepared by sequential grinding with emery papers of decreasing grit sizes, rinsed with distilled water, and mounted in epoxy resin to expose a 1 cm^2 working area as the working electrode. All experiments were performed in naturally aerated, unstirred solutions at room temperature (25 °C). Prior to each measurement, the working electrode was allowed to stabilize freely for 3600 s (1 hour) to attain a stable open-circuit potential (OCP), denoted as the corrosion potential (Ecorr). Potentiodynamic polarization (PDP) scans were then recorded by sweeping the potential from −500 mV to +500 mV relative to the OCP at a scan rate of 1 mV/s (0.001 V/s), covering both cathodic and anodic regions. Electrochemical impedance spectroscopy (EIS) was additionally employed to probe the reaction kinetics, interfacial properties at the metal–electrolyte interface, and the protective influence of the NBL extract on corrosion processes. EIS measurements were performed at the OCP using a small sinusoidal perturbation of 10 mV (rms) over a frequency range from 100 kHz to 100 mHz. Inhibition efficiencies were subsequently determined from the PDP and EIS data using Equations 5 and 6, respectively [39, 40].

$$\text{IE } \% = \left(1 - \frac{I^{i}_{corr}}{I^{o}_{corr}}\right) \times 100$$

$$\text{IE } \% = \left(1 - \frac{R^{o}_{ct}}{R^{i}_{ct}}\right) \times 100$$

2.9.1. Were

- I_CORR^O = corrosion current density when no inhibitor is applied,
- I_CORR^I = corrosion current density when the inhibitor is applied,
- R_CT^O = charge transfer resistance when no inhibitor is applied,
- R_CT^I = charge transfer resistance when the inhibitor is applied.

3. Results And Discussions

3.1. Characterization Result of AISI 4140 Alloy Steel Tubing

The elemental compositions of the AISI 4140 coupon as determined with AES are presented in Table 3. According to the data in Table 3, the AISI 4140 steel coupon comprises approximately 97.24% iron (Fe), rendering it highly susceptible to corrosion in aggressive environments, such as the hydrochloric acid (HCl) medium employed in this study.

Table 3 Elemental compositions of AISI 4140 steel Coupon

Elements	**Fe (%)**	**C (%)**	**Si (%)**	**Mn (%)**	**P (%)**	**S (%)**	**Cr (%)**	**Ni (%)**	**Mo (%)**
%	97.24	0.3679	0.1414	0.5926	<0.02	0.0475	0.7436	0.0773	<0.01
Elements	Cu (%)	Al (%)	Ti (%)	V (%)	Co (%)	Nb (%)	W (%)	Sn (%)	C.E (%)
%	0.3473	0.0522	0.0037	0.0251	<0.004	0.0237	<0.05	>0.1	0.69.02

3.2. Qualitative and Quantitative Phytochemical Analysis Results of NBL

The phytochemical analysis of NBL leaf extract revealed the presence of several bioactive compounds, both qualitatively and quantitatively, as shown in Table 4.

Table 4 Phytochemical analysis result of NBL

Phytochemicals	Qualitative Result (+ means presence & - means absence)	Quantitative (using 1g)
Saponins	-	-
Alkaloids	-	-
Flavonoids	+	0.00712g
Phenols	+	0.00481g
Tannins	+	0.00617g
Steroids	+	0.00243g
Terpenes	+	0.00317g
Glycosides	+	0.00617g

The results indicated tannins, flavonoids, steroids, glycosides, terpenoids, and phenols. Flavonoids were the most abundant, suggesting a significant role in corrosion inhibition due to their ability to form stable complexes with metal surfaces through oxygen-containing functional groups and π-electron systems [41]. Tannins and glycosides, present in comparable quantities, likely contribute to inhibition by forming protective films via adsorption and complexation with iron ions [21, 24]. Phenols, with moderate content, enhance antioxidant properties, reducing oxidative corrosion processes [27]. Terpenoids and steroids, though less abundant, may support inhibition through hydrophobic interactions that repel corrosive species. These phytochemicals collectively facilitate the adsorption of NBL extract onto the AISI 4140 steel surface, forming a protective barrier against the aggressive HCl environment. The quantitative distribution underscores the synergistic effect of these compounds, with flavonoids and tannins playing dominant roles in the inhibition mechanism, as their heteroatoms and aromatic structures promote strong chemisorption and physisorption.

3.3. Process Modeling and Optimization via RSM-OCD

Tables 5 and 6, respectively, show the ANOVA for CR and IE factors. From Table 5, it can be deduced that the independent factors- immersion time, inhibitor concentration, and temperature had significant effects on CR, with factor interaction effects between time and inhibitor concentration (AB), time and temperature (AC), and inhibitor concentration and temperature (BC). These individual and factor interactive effects on CR are significant as shown by their respective p-values, which were all less than 0.05 using a confidence interval of 95% (significance value, α=5%).

Table 5 Analysis of variance (ANOVA) for the CR factor

Source	Sum of Squares	DF	Mean Square	F-value	p-value	
Model	636.71	14	45.48	8601.87	0.0085	significant
A-Time	50.73	1	50.73	9595.10	0.0065	
B-NBL concentration	33.07	2	16.54	3127.65	0.0126	
C-Temperature	463.60	2	231.80	43842.59	0.0034	
AB	11.04	2	5.52	1043.59	0.0219	
AC	13.11	2	6.56	1240.07	0.0201	
BC	6.04	4	1.51	285.51	0.0444	
A^2	0.5826	1	0.5826	110.18	0.0605	
Residual	0.0053	1	0.0053			
Cor Total	636.71	15				

Table 6 Analysis of variance (ANOVA) for IE factor

Source	Sum of Squares	DF	Mean Square	F-value	p-value	
Model	1449.98	5	290.00	109.33	< 0.0001	significant
A-Time	122.44	1	122.44	46.16	< 0.0001	
B-NBL concentration	119.51	2	59.76	22.53	0.0002	
C-Temperature	1093.86	2	546.93	206.19	< 0.0001	
Residual	26.53	10	2.65			
Cor Total	1476.51	15				

Additionally, all the considered independent factors had significant effects on the inhibition efficiency (IE), with no significant interactive effects, as confirmed by P-values below 0.05 in Table 6. Figures 5–7 show the plots of the desirability function, corrosion rate (CR), and inhibition efficiency (IE), respectively, as functions of time, NBL concentration, and process temperature. The optimal solution from the RSM-OCD was obtained at a desirability value of 1.0, corresponding to the following independent factor levels: time = 2 h, NBL concentration = 6 g/L, and temperature = 303 K. At this optimal point, the predicted response values were CR = 1.256 mm/yr and IE = 94.056%. These results indicate that lower exposure time and process temperature, combined with higher inhibitor concentration, increase IE while reducing CR. The optimal points are also illustrated in Figures 6 and 7, along with the predicted response surfaces. Furthermore, Figure 6 shows that CR increases with increasing time and temperature but decreases with increasing inhibitor concentration. Similarly, Figure 7 reveals that IE decreases as time and temperature increase but rises with increasing inhibitor concentration. This behavior of the NBL inhibitor strongly suggests physisorption characteristics, as inhibition efficiency typically decreases with rising temperature in physisorption-dominated systems. Therefore, the NBL inhibitor performs most effectively under conditions of low temperature and short exposure time, combined with higher concentrations although the use of higher inhibitor concentrations may present economic disadvantages.

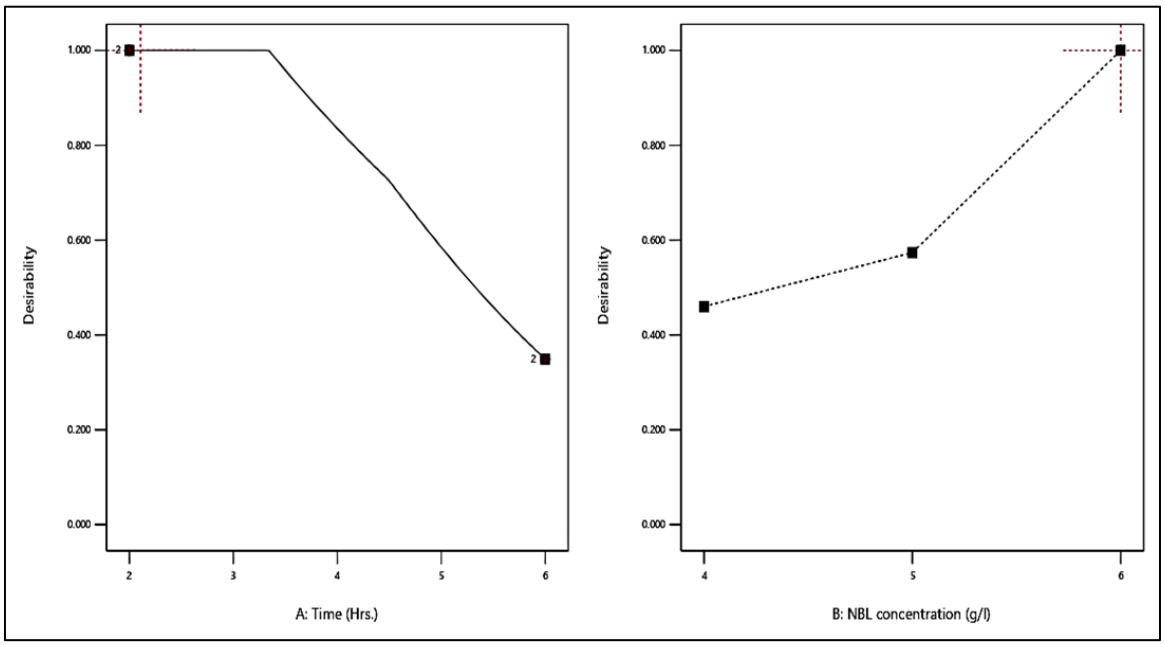

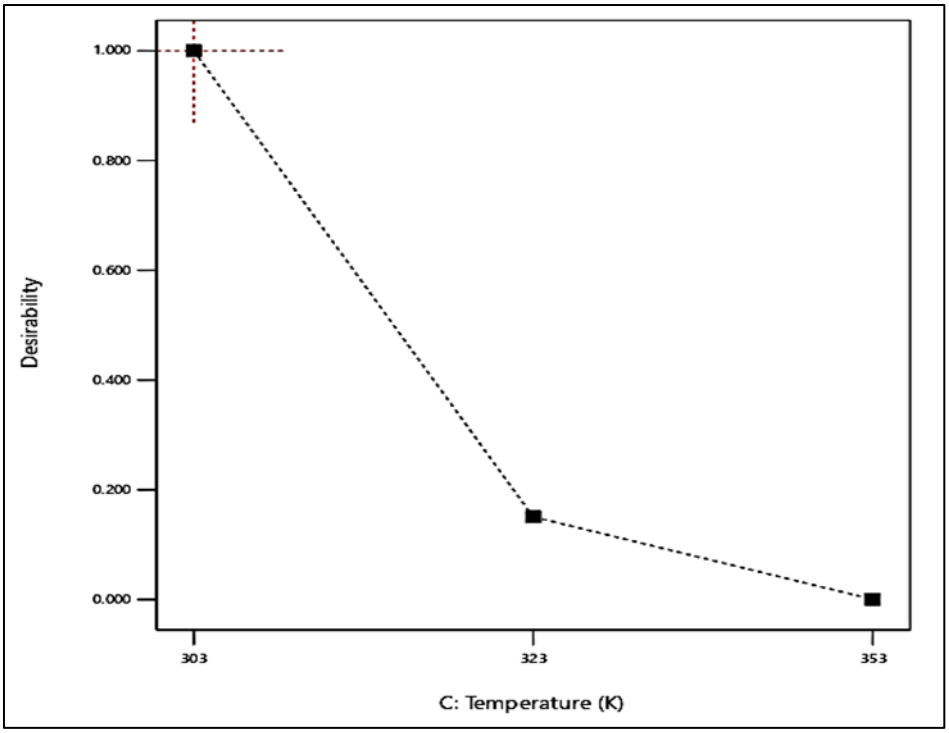

Figure 5 Desirability function plot for (a) time, (b) NBL concentration, and (c) temperature

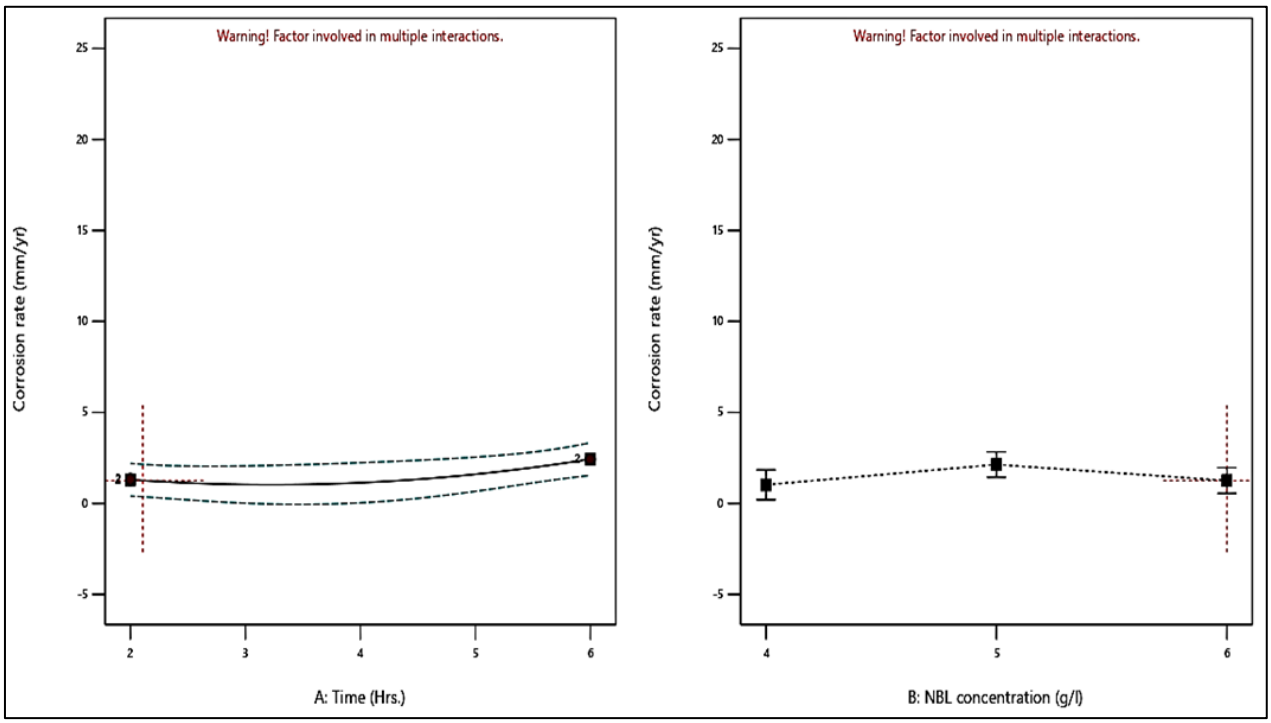

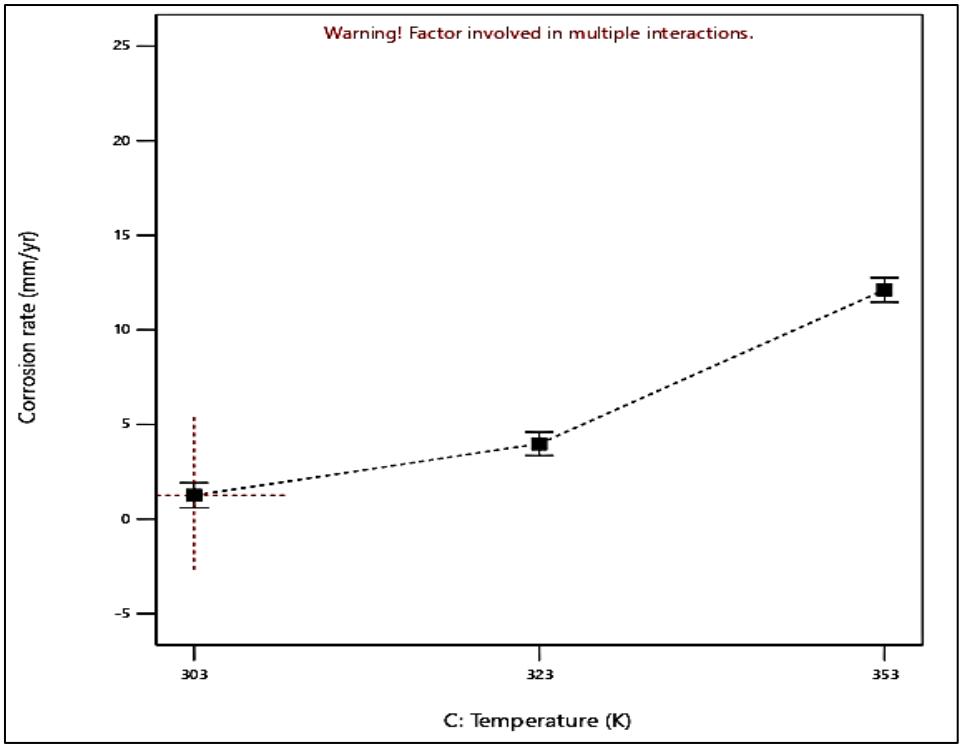

Figure 6 Plot of CR against (a) time, (b) NBL concentration, (c) temperature

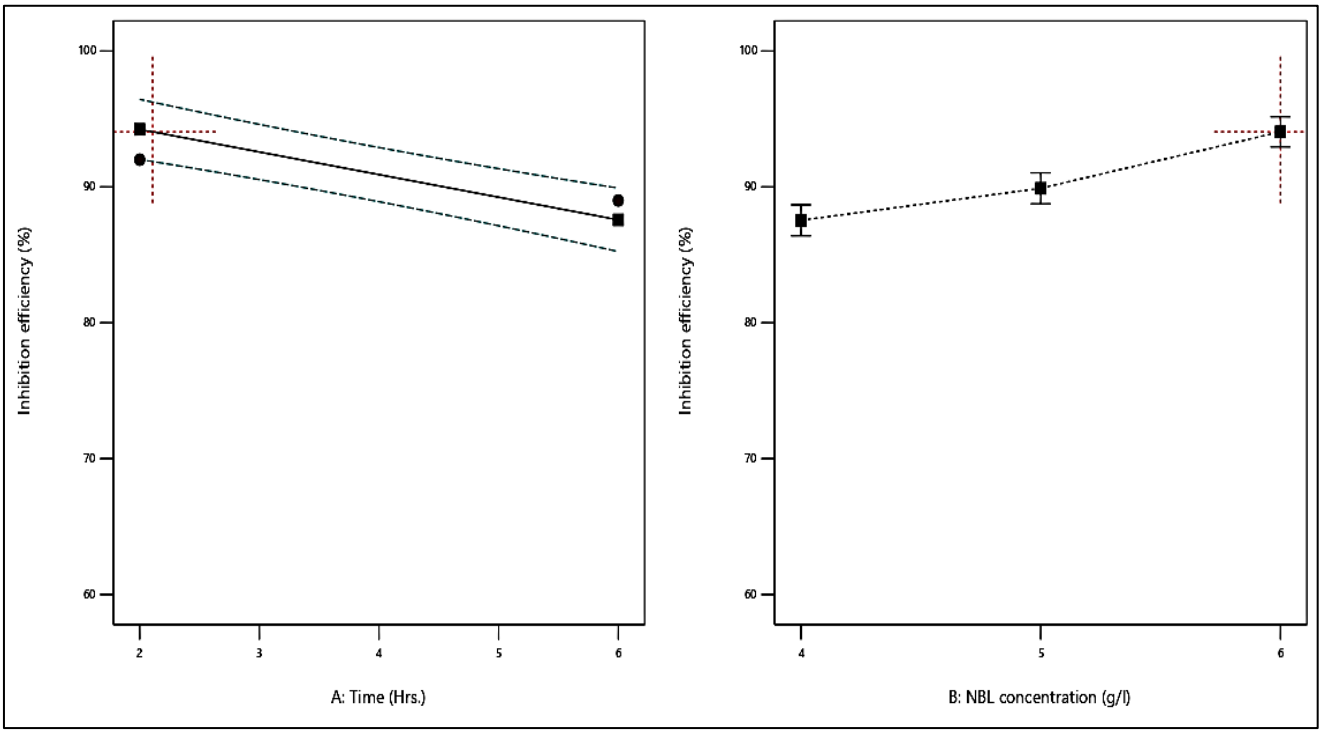

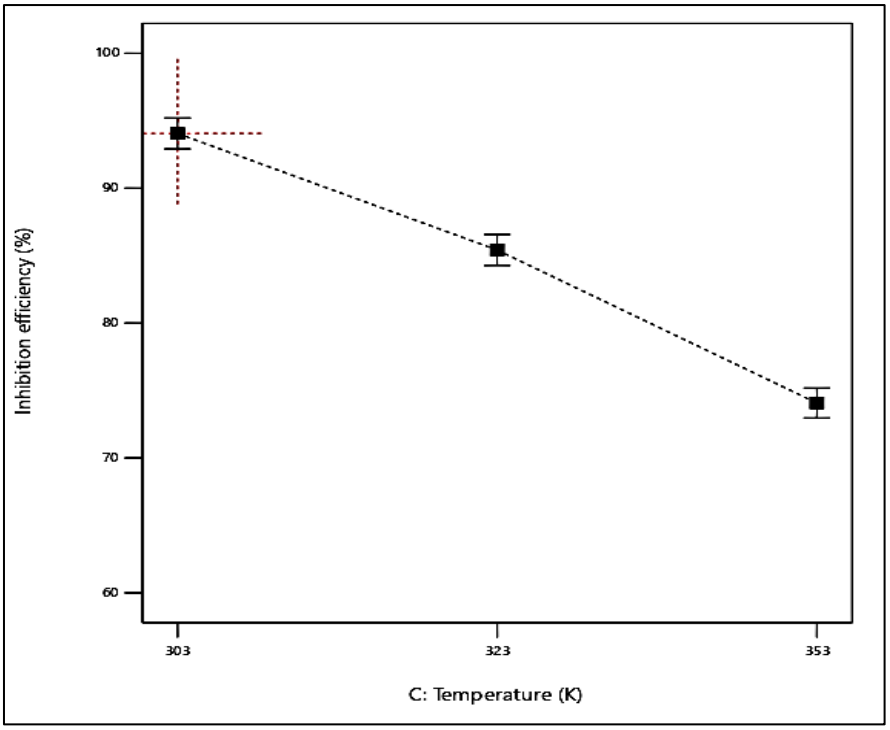

Figure 7 Plot of IE against (a) time, (b) NBL concentration, (c) temperature

3.4. Electrochemical Measurement Results

3.4.1. Potentiodynamic Polarization (PDP)

The PDP parameter for AISI 4140 alloy steel in 15% HCl, with and without NBL inhibitor are summarized in Table 7, while the corresponding Tafel plot is depicted in Figure 8. Based on Table 7, the corrosion current density (Icorr) decreases markedly with rising NBL concentration, from 37.23 μA/cm^2 in the blank (0 g/L) to 3.94 μA/cm^2 at 7 g/L. This decline signifies reduced corrosion kinetics, attributed to the adsorption of NBL's phytochemical constituents onto the steel surface, forming a barrier that hinders electron transfer and corrosive ion access [39, 42]. The inhibition efficiency (IE) increased from 77.41% at 4 g/L to 89.42% at 7 g/L, demonstrating concentration-dependent protection typical of green inhibitors [33].

Table 7 Potentiodynamic Polarization (PDP) result of AISI 4140 coupon in 15% HCl with and without NBL inhibitor

System (15% HCl)	ECORR (mV)	ICORR (μA/cm^2)	β_a(V/dec)	-β_c(V/dec)	θ	IE (%)
Blank	-832	37.23	0.358	0.722	-	-
4g/l of TA	-942	8.41	0.221	0.612	0.7352	77.41
5g/l of TA	-961	6.51	0.116	0.587	0.8252	82.51
6g/l of TA	-978	5.13	0.088	0.564	0.8622	86.22
7g/l of TA	-987	3.94	0.061	0.546	0.8942	89.42

Additionally, the corrosion potential (Ecorr) shifts cathodically from -832 mV (blank) to -987 mV at 7 g/L, indicating preferential suppression of the cathodic hydrogen evolution reaction [43]. Nonetheless, reductions in both anodic (βa, from 0.358 V/dec to 0.061 V/dec) and cathodic (βc, from 0.722 V/dec to 0.546 V/dec) Tafel slopes suggest NBL functions as a mixed-type inhibitor, modulating both anodic metal dissolution and cathodic processes (that is hydrogen evolution) [44].

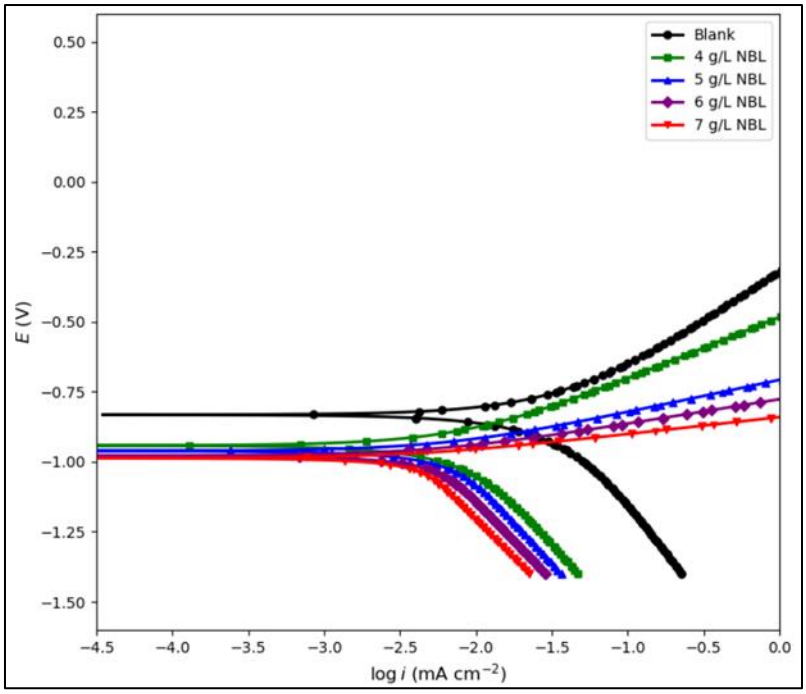

Figure 8 Tafel polarization plot of AISI 4140 coupon in 15% HCl with and without NBL inhibitor

In Fig. 8, the Tafel plots exhibit a progressive shift of polarization curves to lower current densities and more negative potentials with higher NBL concentrations, without altering the curve shapes, implying unchanged reaction mechanisms but effective site-blocking adsorption [39]. The steeper anodic branches at elevated concentrations align with the diminished βa values in Table 7, confirming enhanced anodic inhibition alongside cathodic dominance.

3.4.2. Electrochemical Impedance Spectroscopy (EIS)

The equivalent electrical circuit employed for interpreting the electrochemical impedance spectroscopy (EIS) results consists of the solution resistance (Rs), charge transfer resistance (RCT), inductive resistance (RL), and a constant phase element (CPE), as illustrated in Fig. 9. The impedance of the CPE follows a capacitive formulation, except that its phase angle remains independent of frequency, as expressed in Equation (6).

$$Z_{CPE} = \frac{1}{Q_o(j\omega)^n}$$

Where: Qo = the constant phase element (CPE) with the numerical value of admittance, n = an exponent ranging from −1 to 1. Specifically, when n = -1, 1/QO corresponds to inductance; when n=0, QO equals admittance and indicates low surface inhomogeneity; when n = 0.5, ZCPE represents the Warburg impedance; and when n = 1, Qo corresponds to capacitance. The term j = the imaginary unit.

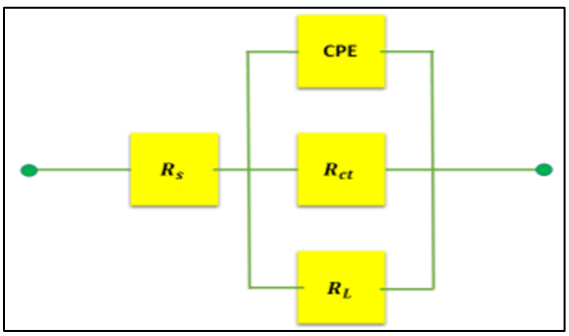

Figure 9 The equivalent circuit used in fitting the electrochemical impedance data

The double layer capacitance was computed using equation 7.

$$C_{dl} = \frac{1}{2\pi f_{max}\left(\frac{R_{ct}R_L}{R_{ct}+R_L}\right)}$$

Where f_{max} = the frequency corresponding to the maximum imaginary impedance.

The EIS study provided quantitative insight into the interfacial adsorption and protective film formation by NBL inhibitor during the steel corrosion in 15% HCl. The fitted parameters are summarized in Table 8, while the corresponding Nyquist plots are shown in Figure 10. The Nyquist spectra shown in Figure 10 consist of single depressed semicircular arcs for both blank and inhibited systems, confirming that corrosion remains under charge-transfer control without change in the fundamental mechanism upon NBL addition. The capacitive loop diameter enlarges markedly with increasing NBL concentration, attaining the largest size at 7 g/L. This visual progression aligns precisely with the charge-transfer resistance (RCT) values in Table 8, which rise from 412.7 Ω·cm^2 (blank) to 3530.37 Ω·cm^2 at 7 g/L NBL. Such increase demonstrates the successful adsorption of NBL phytoconstituents, forming a compact barrier layer that blocks active sites and retards electron transfer [33].

Table 8 The EIS results of corrosion action of AISI 4140 coupon in 15% HCl with and without NBL inhibitor

System (in 15% HCl)	R_s ($\Omega.cm^2$)	R_L ($\Omega.cm^2$)	R_{ct} ($\Omega.cm^2$)	n	C_{dl} ($\mu F.cm^{-2}$)	θ	IE (%)
Blank	2.02	6.28	412.7	0.871	40.80	-	-
4g/l of TA	2.26	177.12	1693.48	0.916	31.12	0.7563	75.63
5g/l of TA	2.20	456.43	2044.08	0.938	19.54	0.7981	79.81
6g/l of TA	2.53	398.20	2834.48	0.946	11.32	0.8544	85.44
7g/l of TA	2.74	488.04	3530.37	0.957	4.26	0.8831	88.31

In addition, the double-layer capacitance (Cdl) decreases sharply from 40.80 μF·cm^{-2} (blank) to 4.26 μF·cm^{-2} at 7 g/L, attributed to the replacement of water and aggressive ions by larger, less dielectric inhibitor molecules, thereby thickening the electrical double layer [39]. The increase in the constant-phase element exponent n (from 0.871 to 0.957) further indicates improved surface homogeneity and reduced roughness due to uniform inhibitor coverage [44]. Inhibition efficiency derived from Rct reaches a maximum of 88.31% at 7 g/L, corroborating the PDP results and confirming the concentration-dependent, adsorption-driven performance of NBL. The slight rise in solution resistance (Rs) and pronounced increase in RL reinforce the development of a stable protective film at the metal–electrolyte interface. Figure 11 clearly delineates the Bode plots, which corroborate the foregoing discussions.

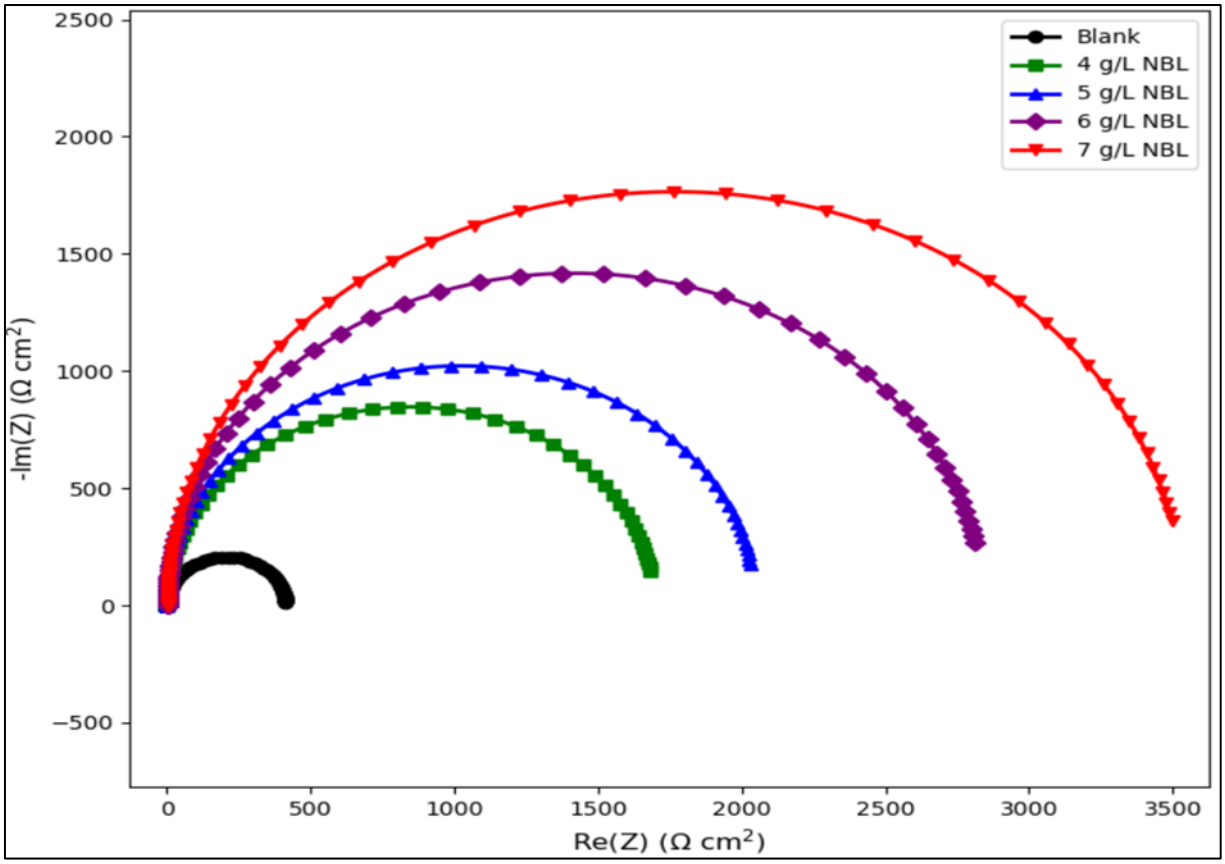

Figure 10 Nyquist plot for AISI 4140 alloy steel in 15% HCl with and without NBL inhibitor

The magnitude plot (shown on the left-side plot), the low-frequency impedance modulus (|Z|) increases markedly with NBL concentration, attaining the highest value at 7 g/L. This steady increase directly corresponds to the rise in Rct from 412.7 $\Omega \cdot cm^2$ (blank) to 3530.37 $\Omega \cdot cm^2$ (7 g/L) and the parallel reduction in Icorr, confirming the progressive build-up of a highly resistive protective film by adsorbed NBL phytoconstituents [39]. Also, for the phase-angle plot (shown on the right-side of plot), the maximum phase angle increases and approaches closer to 90° while the phase peak broadens with rising NBL concentration. This behavior reflects a transition to a more ideal capacitive response, indicating the formation of a thicker, denser, and less defective adsorbed layer that effectively impedes charge transfer and enhances surface homogeneity [39, 44]. The trend aligns precisely with the increase in CPE exponent n (from 0.871 to 0.957) and the sharp drop in Cdl (40.80 to 4.26 $\mu F \cdot cm^{-2}$) reported in Table 8.

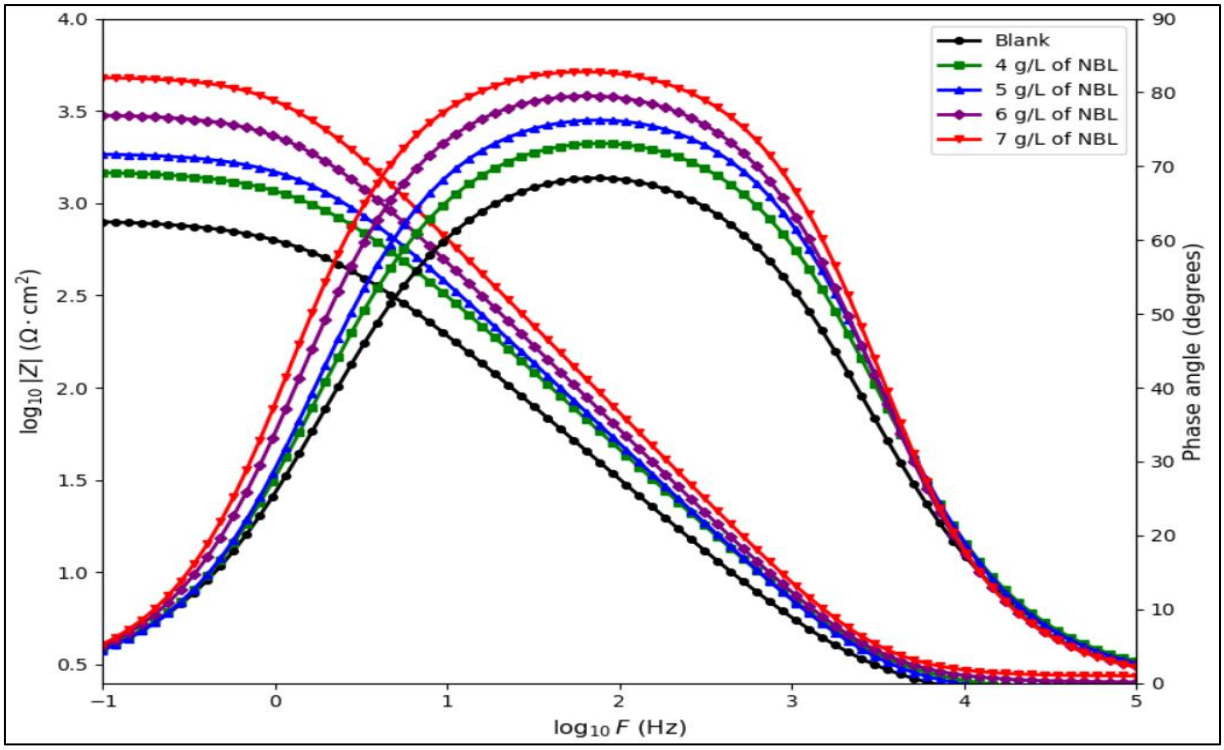

Figure 11 Bode plot for AISI 4140 alloy steel in 15% HCl with and without NBL inhibitor

Therefore, the Bode results reinforce that NBL functions as an efficient mixed-type green inhibitor, delivering concentration-dependent protection up to 89.42 % (PDP) and 88.31 % (EIS) through strong adsorption without altering the underlying corrosion mechanism.

3.5. Surface Characterization

The SEM micrographs at 300× magnification in Figure 12 provide direct physical evidence of the corrosion inhibition by 6 g/l of NBL on AISI 4140 alloy steel after 6 h immersion in 15% HCl at 353 K. Figure 12a shows the as-received polished surface with a smooth and uniform morphology revealing the internal build of the steel. Also, in the absence of NBL inhibitor as shown in Figure 12b, the surface suffers severe degradation characterized by deep cracks, extensive pitting, and a highly rough, porous texture, confirming aggressive acid attack on the unprotected steel. But with the addition of 6 g/l of NBL as presented in Figure 12c, the surface showed evidence of layer coverage by a dense, heterogeneous protective film (NBL Protective layers). This adsorbed layer effectively shields the substrate, substantially reducing the cracks and pits observed in the blank specimen. This observation is in firm agreement with the reports of [39, 45, 46]. These morphological changes offer compelling visual confirmation of the adsorption-driven mechanism established from PDP (mixed-type behavior, IE% up to 89.42%) and EIS (increased Rct up to 3530.37 $\Omega \cdot cm^2$, decreased Cdl , IE% = 88.31%), demonstrating that NBL phytochemicals form a stable barrier film that retards corrosive attack without altering the underlying mechanism.

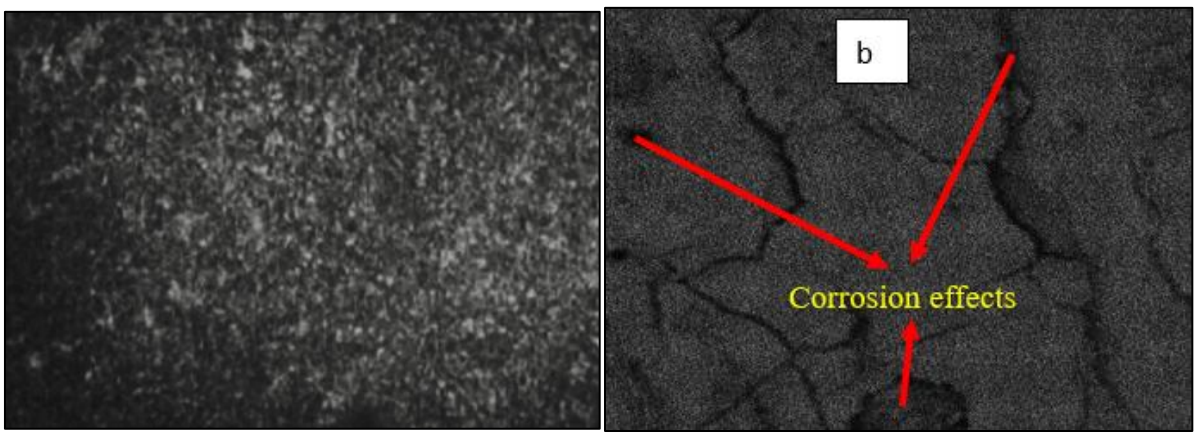

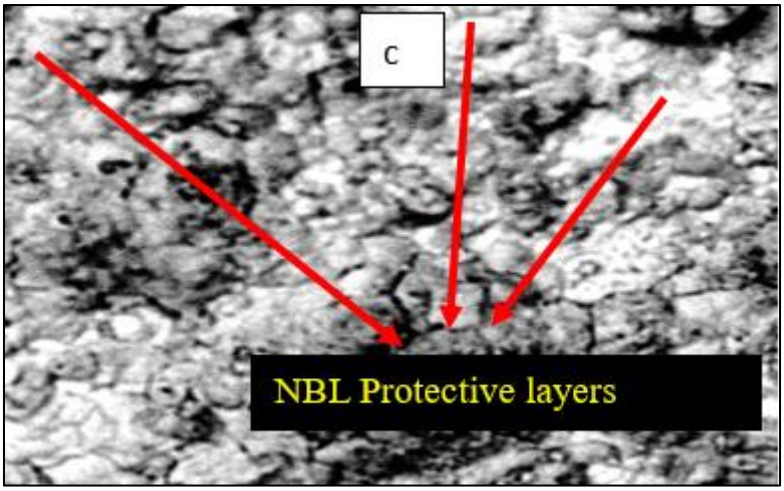

Figure 12 SEM at 300× for (a) the as-received AISI 4140 alloy steel coupon, (b) sample immersed in 15% HCl without NBL inhibitor at the conditions of 353K and 6hrs. immersion time, (c) sample immersed in 15% HCl with 6g/l of NBL inhibitor at the conditions of 353K and 6hrs. immersion time

4. Conclusions and Direction for Future Studies

The primary objective of this investigation was to evaluate the corrosion inhibition performance of NBL leaf extract on AISI 4140 alloy steel in 15% HCl, the aggressive medium typically employed during oil and gas well acidizing operations, and to systematically optimize the key process parameters (immersion time, inhibitor concentration, and temperature) using the RSM-OCD approach. This study successfully demonstrated the potential of NBL leaf extract as an efficient, sustainable, and eco-friendly green corrosion inhibitor that offers a viable alternative to conventional synthetic inhibitors while deepening the mechanistic understanding of bio-based corrosion protection. The key findings are summarized as follows

- RSM-OCD optimization identified the optimal conditions as 2 h immersion time, 6 g/L NBL concentration, and 303 K temperature, with predicted corrosion rate of 1.256 mm/yr. and inhibition efficiency of 94.056%.
- Potentiodynamic polarization studies confirmed NBL as a mixed-type inhibitor, with corrosion current density decreasing from 37.23 μA/cm^2 (blank) to 3.94 μA/cm^2 at 7 g/L, inhibition efficiency reaching 89.42%, and a cathodic shift in corrosion potential from -832 mV to -987 mV.
- Electrochemical impedance spectroscopy results showed single depressed semicircular arcs, with charge-transfer resistance increasing from 412.7 Ω·cm^2 (blank) to 3530.37 Ω·cm^2 at 7 g/L, double-layer capacitance decreasing from 40.80 μF·cm^{-2} to 4.26 μF·cm^{-2}, CPE exponent n increasing from 0.871 to 0.957, and inhibition efficiency of 88.31%.
- SEM micrographs at 300× revealed severe degradation with deep cracks, pitting, and rough porous texture in the blank specimen after 6 h at 353 K, while the surface with 6 g/L NBL exhibited markedly smoother morphology covered by a dense heterogeneous protective film.
- Phytochemical analysis identified flavonoids (0.00712 g), phenols (0.00481 g), tannins (0.00617 g), steroids (0.00243 g), terpenoids (0.00317 g), and glycosides (0.00617 g) as the bioactive constituents responsible for adsorption-driven inhibition.
- ANOVA confirmed that immersion time, NBL concentration, temperature, and their interactions (AB, AC, BC) had significant effects on corrosion rate and inhibition efficiency ($p < 0.05$).

However, future investigations should integrate advanced machine learning algorithms with the RSM-OCD framework to enhance predictive accuracy and should conduct field trials under actual oil and gas well acidizing conditions to deepen mechanistic understanding and accelerate the adoption of this bio-based corrosion inhibitor.

Compliance with ethical standards

Acknowledgments

The authors are deeply grateful to the Tertiary Education Trust Fund (TET Fund), Nigeria, and Imo State University, Owerri, Nigeria, for the full financial sponsorship of this research through the Institution-Based Research (IBR) grant. This generous support covered all aspects of the study, including procurement of materials, laboratory analyses, equipment usage, and fieldwork, thereby making the successful completion of the project possible. The TET Fund's funding has been invaluable in promoting eco-friendly corrosion inhibition research with direct relevance to the Nigerian oil and gas industry.

Disclosure of conflict of interest

No conflict of interest to be disclosed.

Data availability statement

The data used for study will be available upon reasonable request.

Statement of informed consent

Informed consent was not required for this study because no human participants or personal data were involved.

References

[1] L. L. Machuca, K. Lepkova, and A. Petroski, "Corrosion of carbon steel in the presence of oilfield deposit and thiosulphate-reducing bacteria in CO 2 environment," Corrosion Science, vol. 129, pp. 16–25, Dec. 2017, doi: 10.1016/j.corsci.2017.09.011.

[2] [2]K. Azzaoui et al., "Eco friendly green inhibitor Gum Arabic (GA) for the corrosion control of mild steel in hydrochloric acid medium," Corrosion Science, vol. 129, pp. 70–81, Dec. 2017, doi: 10.1016/j.corsci.2017.09.027.

[3] D. A. Winkler, M. Breedon, P. White, A. E. Hughes, E. D. Sapper, and I. Cole, "Using high throughput experimental data and in silico models to discover alternatives to toxic chromate corrosion inhibitors," Corrosion Science, vol. 106, pp. 229–235, May 2016, doi: 10.1016/j.corsci.2016.02.008.

[4] O. Benali, C. Selles, and R. Salghi, "Inhibition of acid corrosion of mild steel by Anacyclus pyrethrum L. extracts," Research on Chemical Intermediates, vol. 40, no. 1, pp. 259–268, Dec. 2012, doi: 10.1007/s11164-012-0960-8.

[5] S. Karthikeyan, "Drugs as Corrosion Inhibitors: A Review," International Journal of Science and Research (IJSR), vol. 5, no. 4, pp. 671–677, Apr. 2016, doi: 10.21275/v5i4.nov162623.

[6] Z. Sanaei, G. Bahlakeh, and B. Ramezanzadeh, "Active corrosion protection of mild steel by an epoxy ester coating reinforced with hybrid organic/inorganic green inhibitive pigment," Journal of Alloys and Compounds, vol. 728, pp. 1289–1304, Dec. 2017, doi: 10.1016/j.jallcom.2017.09.095.

[7] R. Solmaz, G. Kardaş, B. Yazıcı, and M. Erbil, "Adsorption and corrosion inhibitive properties of 2-amino-5-mercapto-1,3,4-thiadiazole on mild steel in hydrochloric acid media," Colloids and Surfaces A: Physicochemical and Engineering Aspects, vol. 312, no. 1, pp. 7–17, Jan. 2008, doi: 10.1016/j.colsurfa.2007.06.035.

[8] Z. Tao, W. He, S. Wang, S. Zhang, and G. Zhou, "A study of differential polarization curves and thermodynamic properties for mild steel in acidic solution with nitrophenyltriazole derivative," Corrosion Science, vol. 60, pp. 205–213, Jul. 2012, doi: 10.1016/j.corsci.2012.03.035.

[9] K. R. Ansari, M. A. Quraishi, and A. Singh, "Chromenopyridin derivatives as environmentally benign corrosion inhibitors for N80 steel in 15% HCl," Journal of the Association of Arab Universities for Basic and Applied Sciences, vol. 22, no. 1, pp. 45–54, Feb. 2017, doi: 10.1016/j.jaubas.2015.11.003.

[10] R. T. R. Carvalho, P. F. Oliveira, L. C. M. Palermo, A. A. G. Ferreira, and C. R. E. Mansur, "Prospective acid microemulsions development for matrix acidizing petroleum reservoirs," Fuel, vol. 238, pp. 75–85, Feb. 2019, doi: 10.1016/j.fuel.2018.10.003.

[11] K. R. Ansari, D. S. Chauhan, A. Singh, V. S. Saji, and M. A. Quraishi, "Corrosion Inhibitors for Acidizing Process in Oil and Gas Sectors," Corrosion Inhibitors in the Oil and Gas Industry, pp. 151–176, Feb. 2020, doi: 10.1002/9783527822140.ch6.

[12] A. O. James and N. B. Iroha, "New green inhibitor of Olax subscorpioidea root for J55 carbon steel corrosion in 15% HCl: theoretical, electrochemical, and surface morphological investigation," Emergent Materials, vol. 5, no. 4, pp. 1119–1131, Feb. 2021, doi: 10.1007/s42247-021-00161-1.

[13] D. Wang, Y. Li, T. Chang, and A. Luo, "Experimental and theoretical studies of chitosan derivatives as green corrosion inhibitor for oil and gas well acid acidizing," Colloids and Surfaces A: Physicochemical and Engineering Aspects, vol. 628, p. 127308, Nov. 2021, doi: 10.1016/j.colsurfa.2021.127308.

[14] Y. Zhao et al., "Investigation of the failure mechanism of the TG-201 inhibitor: Promoting the synergistic effect of HP-13Cr stainless steel during the well completion," Corrosion Science, vol. 166, p. 108448, Apr. 2020, doi: 10.1016/j.corsci.2020.108448.

[15] J. Zang, C. Yin, Z. Bai, Y. Feng, Y. Wang, and M. Wu., "Corrosion inhibition mechanism of the TG 201 acid corrosion inhibitor on N80 and HP13Cr steel," Proceedings of the 16th National Symposium on corrosion inhibitors, The 16th National corrosion inhibitor Academic Discussion and Application Technology Experience Exchange Meeting, 2010, July 28, Shaghai, China., 2010.

[16] M. Finšgar and J. Jackson, "Application of corrosion inhibitors for steels in acidic media for the oil and gas industry: A review," Corrosion Science, vol. 86, pp. 17–41, Sep. 2014, doi: 10.1016/j.corsci.2014.04.044.

[17] L. Guo, C. Qi, X. Zheng, R. Zhang, X. Shen, and S. Kaya, "Toward understanding the adsorption mechanism of large size organic corrosion inhibitors on an Fe(110) surface using the DFTB method," RSC Advances, vol. 7, no. 46, pp. 29042–29050, 2017, doi: 10.1039/c7ra04120a.

[18] Z. Cao, Y. Tang, H. Cang, J. Xu, G. Lu, and W. Jing, "Novel benzimidazole derivatives as corrosion inhibitors of mild steel in the acidic media. Part II: Theoretical studies," Corrosion Science, vol. 83, pp. 292–298, Jun. 2014, doi: 10.1016/j.corsci.2014.02.025.

[19] L. Guo et al., "Theoretical insight into an empirical rule about organic corrosion inhibitors containing nitrogen, oxygen, and sulfur atoms," Applied Surface Science, vol. 406, pp. 301–306, Jun. 2017, doi: 10.1016/j.apsusc.2017.02.134.

[20] G. Sığırcık, T. Tüken, and M. Erbil, "Assessment of the inhibition efficiency of 3,4-diaminobenzonitrile against the corrosion of steel," Corrosion Science, vol. 102, pp. 437–445, Jan. 2016, doi: 10.1016/j.corsci.2015.10.036.

[21] K. Rashed, "Phytochemical and Biological Effects of Newbouldiaia laevis : A Review," Plantae Scientia, vol. 4, no. 5, pp. 208–213, Sep. 2021, doi: 10.32439/ps.v4i5.208-213.

[22] A. Espinoza-Vázquez et al., "Adsorption and corrosion inhibition behaviour of new theophylline–triazole-based derivatives for steel in acidic medium," Royal Society Open Science, vol. 6, no. 3, p. 181738, Mar. 2019, doi: 10.1098/rsos.181738.

[23] Z. Salarvand, M. Amirnasr, M. Talebian, K. Raeissi, and S. Meghdadi, "Enhanced corrosion resistance of mild steel in 1M HCl solution by trace amount of 2-phenyl-benzothiazole derivatives: Experimental, quantum chemical calculations and molecular dynamics (MD) simulation studies," Corrosion Science, vol. 114, pp. 133–145, Jan. 2017, doi: 10.1016/j.corsci.2016.11.002.

[24] N. Amandine et al., "Phytochemical Screening and Antimicrobial Properties of Leaf Extracts from Newbouldiaia laevis (P. Beauv) and Flueggea virosa (Roxb. ex Willd.)," Science Journal of Chemistry, vol. 13, no. 2, pp. 33–40, Apr. 2025, doi: 10.11648/j.sjc.20251302.11.

[25] L.A. Okeke, Clement O.A., D.C. Nwobodo, and V.K. Okolo, "Phytochemical analysis and antibacterial activities of various leaf extracts of Ocimum gratissimum and Newbouldiaia laevis," GSC Biological and Pharmaceutical Sciences, vol. 22, no. 3, pp. 144–152, Mar. 2023, doi: 10.30574/gscbps.2023.22.3.0104.

[26] R. Bansal et al., "Synthesis and Evaluation of a New Series of 8-(2-Nitroaryl)Xanthines as Adenosine Receptor Ligands," Drug Development Research, vol. 77, no. 5, pp. 241–250, Jul. 2016, doi: 10.1002/ddr.21317.

[27] C.N. Obum-Nnadi, F.N. Okey-Ndeche, P.A. Nnagbo, and N.B. Ohabughiro, "Evaluation of the antioxidant and antibacterial activities of Newbouldiaia laevis leaves," International Journal of Green and Herbal Chemistry, vol. 11, no. 1, Apr. 2022, doi: 10.24214/ijghc/hc/11/1/01532.

[28] A. O. Odiongenyi, S. A. Odoemelam, and N. O. Eddy, "Corrosion Inhibition and Adsorption Properties of Ethanol Extract of Vernonia Amygdalina for the Corrosion of Mild Steel in H2SO4," Portugaliae Electrochimica Acta, vol. 27, no. 1, pp. 33–45, 2009, doi: 10.4152/pea.200901033.

[29] D. I. Oraekei, S. I. Mbagwu, and K. E. Iduma, "Evaluation of the pharmacological interactions between coadministered Newbouldiaia laevis root bark extract and omeprazole in ulcer induced rat model," Journal of Current Biomedical Research, vol. 2, no. 6, November-December, pp. 659–667, Dec. 2022, doi: 10.54117/jcbr.v2i6.7.

[30] Y.B. Waidi, B. Nkoi, R.K.C. Amadi, and A.A. Luke, "Determination of the Effect of Newbouldiaia Leavis Leaf Extract on the Corrosion of Mild Steel in Sulphuric Acid," Journal of Newviews in Engineering and Technology (JNET), vol. 2, no. 1, pp. 9–16, 2020, doi: http://www.rsujnet.org/index.php/publications/2020-edition.

[31] Y.B. Waidi, "Newbouldiaia Laevis Leaf Extract's Possibilities as a Medium Carbon Steel Corrosion Inhibitor in Sulphuric Acid (H2SO4) Using a Weight Loss Technique ," Global Scientific Journals, vol. 10, no. 10, pp. 794–806, 2022.

[32] Y.B. Waidi, A.W. Okpala, and E.A. Ogbonnaya, "The Inhibitory Effect of Ethanolic Extract of Newbouldiaia Laevis Leaf on the Corrosion of High Carbon Steel in 1M Sulphuric Acid (H2SO4)," International Journal of Engineering Research & Technology (IJERT), vol. 11, no. 4, pp. 64–68, 2022. DOI : https://doi.org/10.5281/zenodo.18447906

[33] A.C. Adah, J.A. Gbertyo, and A.G. Otokpa, "Studies on the Corrosion Inhibition of Ethanol Extract of Newbouldiaia Laevis Stem Bark and Leaf on Mild Steel in Acidic Medium," Chemistry Research Journal, vol. 5, no. 2, pp. 96–103, 2020.

[34] C. S. Ezeonu and C. M. Ejikeme, "Qualitative and Quantitative Determination of Phytochemical Contents of Indigenous Nigerian Softwoods," New Journal of Science, vol. 2016, pp. 1–9, Oct. 2016, doi: 10.1155/2016/5601327.

[35] I. Tekam, S. Dubey, S. Mahajan, S. Sheikh, S. M. Singh, and A. Kewat, "Quantitative and qualitative assessment of phytochemicals in Dandelion (Taraxacum officinale) leaves," Journal of Experimental Zoology India, vol. 27, no. 01, Jan. 2024, doi: 10.51470/jez.2024.27.1.699.

[36] A. Altemimi, N. Lakhssassi, A. Baharlouei, D. Watson, and D. Lightfoot, "Phytochemicals: Extraction, Isolation, and Identification of Bioactive Compounds from Plant Extracts," Plants, vol. 6, no. 4, p. 42, Sep. 2017, doi: 10.3390/plants6040042.

[37] A. J. Harborne, Phytochemical Methods A Guide to Modern Techniques of Plant Analysis. Springer Science & Business Media, 1998.

[38] Standard practice for Laboratory immersion corrosion testing of metals, ASTM G31 - 72 (re-approved 2004).

[39] S. C. Udensi, O. E. Ekpe, and L. A. Nnanna, "Newbouldiaia laevis Leaves Extract as Tenable Eco-Friendly Corrosion Inhibitor for Aluminium Alloy AA7075-T7351 in 1 M HCl Corrosive Environment: Gravimetric, Electrochemical and Thermodynamic Studies," Chemistry Africa, vol. 3, no. 2, pp. 303–316, Mar. 2020, doi: 10.1007/s42250-020-00131-w.

[40] A. Hamdy and N. Sh. El-Gendy, "Thermodynamic, adsorption and electrochemical studies for corrosion inhibition of carbon steel by henna extract in acid medium," Egyptian Journal of Petroleum, vol. 22, no. 1, pp. 17–25, Jun. 2013, doi: 10.1016/j.ejpe.2012.06.002.

[41] P. B. Raja and M. G. Sethuraman, "Natural products as corrosion inhibitor for metals in corrosive media: A review," Materials Letters, vol. 62, no. 1, pp. 113–116, Jan. 2008, doi: 10.1016/j.matlet.2007.04.079.

[42] O.M. Chima, E. Ozurumba, L.T. Popoola, F.N. Archibong, O.J. Achalla, & Y.P. Asmara, "Anticorrosion Effect of Pineapple Peel Extract on Mild Steel in Hydrogen Sulfide Environment: Characterization, Optimization and Statistical Analysis via Response Surface Methodology.", Engineering Reports, 7(11): 1-21, 2025. https://doi.org/10.1002/eng2.70445

[43] L.A. Nnanna, V.U. Obasi, O.C. Nwadiuko, K.I. Mejeh, N.D. Ekekwe, & S.C. Udensi, S. C, "Inhibition by Newbouldiaia leavis leaf extract of the corrosion of aluminium in HCl and H2SO4 solutions". Archives of Applied Science Research, 4(1), 207-217, 2012.

[44] S.C. Udensi, O.E. Ekpe, and L.A. Nnanna, "Electrochemical, Gravimetric and Thermodynamic studies of corrosion inhibitive performance of Treculiaafricana on AA7075-T7351 in 1.0 M HCl," Journal of Materials and Environmental Sciences, vol. 10, no. 2, pp. 1272–1285, 2019, doi: http://www.jmaterenvironsci.com/.

[45] N. Chaubey, V. K. Singh, and M. A. Quraishi, "Papaya peel extract as potential corrosion inhibitor for Aluminium alloy in 1 M HCl: Electrochemical and quantum chemical study," Ain Shams Engineering Journal, vol. 9, no. 4, pp. 1131–1140, Dec. 2018, doi: 10.1016/j.asej.2016.04.010.

[46] K. Krishnanjana and G. M. Ganesh, "Punica granatum peel powder and extract as green inhibitor for TMT in 1M HCl: an experimental and response surface model," Green Chemistry Letters and Reviews, vol. 17, no. 1, Oct. 2024, doi: 10.1080/17518253.2024.2412989.